JOURNAL OF GEOPHYSICAL RESEARCH, VOL. 105, NO. D9, PAGES 11,585–11,599, MAY 16, 2000

Impact of acetone on ozone production and OH in the upper troposphere at high NO_x

Ian Folkins
Atmospheric Science Program, Departments of Physics and Oceanography, Dalhousie University Halifax, Nova Scotia, Canada

Robert Chatfield
Earth Science Division, NASA Ames Research Center, Moffett Field, California

Abstract. The impact of acetone (or any HO_x source) on tropospheric photochemistry is largest in the high NO_x regime. The fractional increases in OH and ozone production associated with acetone increase rapidly with NO_x when NO_x mixing ratios become larger than 300 parts per trillion by volume (pptv). This occurs in part because the HO_x yield of acetone is larger at higher NO_x mixing ratios, going from about 1 HO_x at $NO_x \sim 10$ pptv to 3 HO_x at $NO_x \sim 1000$ pptv. We also investigate the effect of acetone on the partitioning of the NO_y family. Acetone increases the conversion of NO to NO_2, HNO_4, HNO_3, and peroxyacetylnitrate (PAN). Conversion of NO to PAN dominates at low NO_x, while conversion of NO to HNO_3 dominates at high NO_x. These NO decreases significantly diminish the increases in OH and ozone production one would otherwise anticipate from the increases in HO_2. In particular, acetone can be expected to reduce ozone production for $NO_x < 25$ pptv. We also show that most of the changes in species concentrations arising from the introduction of a HO_x source can be accurately predicted using simple expressions derived from linear perturbation theory.

1. Introduction

The main source of HO_x ($= OH + HO_2$) in the troposphere is the reaction of O^1D with H_2O, which produces two OH radicals. This source decreases with height due to the rapid decrease of water vapor number densities with altitude. The weakness of this HO_x source in the upper troposphere provides an opportunity for a number of other species to make significant contributions to HO_x production in this region. In particular, there are several chemical species that, although chemically produced near the surface, can be transported into the upper troposphere by deep convection or synoptic systems and which subsequently photolyze to produce HO_x. These HO_x precursors include acetone (CH_3COCH_3), methyl hydroperoxide (CH_3OOH), and possibly formaldehyde (CH_2O).

The vertical transport of HO_x precursors to the upper troposphere [*Chatfield and Crutzen*, 1984] has gained more attention recently due to, among other factors, the realization that acetone is a HO_x source and that its concentration can be quite high in the upper troposphere [*Singh et al.*, 1995; *Arnold et al.*, 1997], that peroxide concentrations in the upper tropical troposphere are much higher than can be explained by steady state models [*Jacob et al.*, 1996; *Jaeglé et al.*, 1997], and the fact that instruments capable of measuring OH and HO_2 in the upper troposphere have been developed and there has been a concerted effort to account for their observed concentrations [*Wennberg et al.*, 1998]. These HO_x sources affect upper tropospheric chemistry in a number of different ways. First, they increase the oxidizing power of the atmosphere by directly increasing OH and HO_2. Second, the higher HO_2 concentrations increase ozone production from the NO + HO_2 reaction [*Prather and Jacob*; 1997, *Folkins et al.*, 1997; *Wennberg et al.*, 1998; *Folkins et al.*, 1998; *Jaeglé et al.*, 1998]. Third, they affect NO_y partitioning by increasing the rate at which NO_x is oxidized to HNO_3 and HNO_4, and in the case of acetone, also to peroxyacetylnitrate (PAN) [*McKeen et al.*, 1997; *Keim et al.*, 1999]. These NO_x decreases offset, to some extent, the increases in ozone production associated with the increases in HO_2. This effect has been examined using a three-dimensional model [*Müller and Brasseur*, 1999].

We examine how the effects of adding acetone to the upper troposphere depend on NO_x. There are several reasons for anticipating that such a dependence might exist. First, the number of HO_x produced during the oxidation of acetone, or any hydrocarbon, should increase with NO_x. Second, while the dominant HO_x loss

Paper number 2000JD900067.
0148-0227/00/2000JD900067$09.00

processes at low NO_x involve reactions between HO_x species (e.g., OH+HO_2 and HO_2+HO_2), the dominant HO_x loss process at high NO_x (OH+NO_2) is linear in HO_x. This should gives rise to some change in the response of HO_x to additional HO_x sources. Finally, the response of HO_x to acetone will be proportional in some sense to the fractional contribution of acetone to the total HO_x production. One of the most important sources of HO_x to the upper troposphere is methane (CH_4) oxidation. This source starts to diminish at high NO_x as OH becomes small, which will increase the relative importance of acetone oxidation to the total HO_x production.

We first introduce a zero-dimensional (point) photochemical model intended to approximate the upper tropical troposphere. (Acetone is also an important HO_x source to the midlatitude upper troposphere, but it is important over a much broader altitude range in the tropics.) There is a prescribed input of convected air into the model each day, and it is run until there is an approximate steady state between the convective forcing and in situ chemistry. After describing some of the baseline chemical characteristics of this model, we introduce acetone into the convected air and examine the resulting fractional changes in OH, HO_2, NO, and NO_2. We show how standard steady state expressions for the partitioning of the HO_x and NO_x families can be used to estimate the fractional changes in these species. We then analyze the HO_x budget to show why the largest fractional changes in OH and HO_2 occur at high NO_x. This analysis requires some method for estimating the HO_x yields of acetone and methane, i.e., the number of HO_x produced by each of these hydrocarbons as they oxidize. It is usually very difficult to calculate HO_x yields of hydrocarbons directly from numerical simulations. We therefore describe a procedure by which the HO_x yields of methane and acetone might be estimated analytically.

The second part of this paper deals with the impact of acetone on ozone production. Acetone increases ozone production by increasing the concentration of HO_2. This is offset by decreases in ozone production associated with the conversion of NO to NO_2, HNO_4, HNO_3, and PAN. We first derive expressions which predict the enhancements in PAN, HNO_3, and HNO_4 associated with the introduction of acetone. These expressions assume that acetone simply moves the concentration of each species from one photochemical steady state to another and that the fractional change in each species is small. After determining how these changes effect NO, we estimate the net impact of acetone on ozone production.

2. Photochemical Model

As was mentioned earlier, the photochemical model is designed to strike a realistic balance in the upper tropical troposphere between the two forcings of convective input and in situ chemistry. It is a modified version of a zero-dimensional photochemical model used in previous studies [*Chatfield et al.*, 1996; *Folkins et al.*, 1998]. The air parcel is at 10 km, near the altitude of maximum convective outflow. The effect of acetone will increase with height from 10 km toward the tropical tropopause. The temperature is 227 K, the water vapor mixing ratio is 100 ppmv, and the surface albedo is 0.1. The effect of convective detrainment is modeled using a replacement time of 15 days. Over the course of a day, the concentration of each species is fractionally reduced by an amount equal to 1/15 and increased by an amount depending on the prescribed properties of convected air. This replacement rate is consistent with those derived from a three-dimensional model [*Prather and Jacob*, 1997]. The model was run until a reasonable steady state balance between convection and in situ chemistry is achieved (here 50 days). The incoming convected air had CO = 60 ppbv, O_3 = 20 ppbv, CH_4 = 1.7 ppmv, and H_2O_2 = CH_3OOH = 50 parts per trillion by volume (pptv), while the concentrations of NO_2, NO_3, N_2O_5, HNO_4, HNO_3, CH_2O, and PAN were all set to zero. The NO mixing ratio of the incoming convected air was varied from 10 to 6000 pptv. Two runs were done for each value of the incoming NO mixing ratio. In the baseline runs, the acetone mixing ratio was set equal to zero, while in the perturbation runs it was set equal to 600 pptv.

Figure 1 gives some indication of the chemical properties of the baseline run. In the lower panel day-averaged HO_2, OH, and O_3 mixing ratios are plotted against the ambient NO_x mixing ratio. The ambient NO_x mixing ratio was less than the NO_x mixing ratio of the incoming convected air because of the conversion, in the model, of NO to other NO_y species.

The upper panel of Figure 1 shows diurnally averaged ozone production rates in the model. The net rate of ozone production in the background troposphere can be written

$$d[O_3]/dt = P(O_3) - D(O_3), \quad (1)$$

where

$$P(O_3) = k_6[NO][HO_2] + k_{10}[NO][CH_3O_2] \quad (2)$$

$$\begin{aligned} D(O_3) &= k_{11}[O^1D][H_2O] \\ &+ k_7[OH][O_3] + k_5[HO_2][O_3]. \end{aligned} \quad (3)$$

Each of these five terms has been plotted against NO_x in the top panel of Figure 1. The largest of the five terms is HO_2+NO (dashed line), which is almost equal to the total dO_3/dt (bold solid line) at all NO_x mixing ratios.

The upper panel of Figure 2 shows the acetone mixing ratio in the model when 600 pptv of acetone is added to the incoming convected air. The resulting ambient acetone mixing ratios of between 290 and 320 pptv are roughly consistent with observed upper tropical tro-

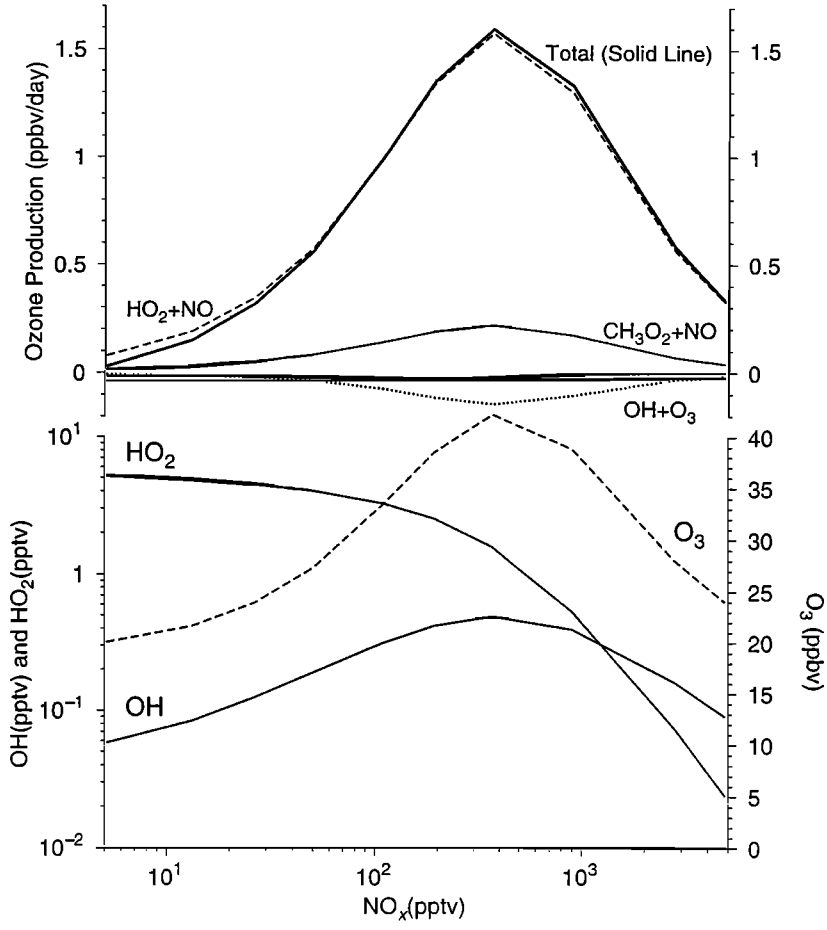

Figure 1. (bottom) Mixing ratios of OH in parts per trillion by volume (pptv), HO_2 (pptv), and O_3 (ppbv) in the baseline model run plotted against NO_x. (top) Ozone production and destruction terms in the baseline model run plotted against NO_x. The two small unlabeled ozone destruction terms are $OH + O_3$ and $O^1D + H_2O$. The dashed line represents ozone production from the $HO_2 + NO$ reaction. The dotted line represents destruction from the $HO_2 + O_3$ reaction. The bold line represents the sum of all five production and destruction terms.

pospheric mixing ratios of between 200 and 450 pptv [*Singh et al.*, 1995]. Although the main sink of acetone in the model is photolysis, OH attack is significant in the range of NO_x mixing ratios at which OH concentrations are largest.

The upper panel of Figure 2 also shows the fractional change of O_3 in going from the baseline to the perturbed simulation (i.e., $d\mathrm{O}_3/\mathrm{O}_3$ = (O_3(acetone) - O_3(baseline))/O_3(baseline)). In contrast to the O_3 mixing ratio, $d\mathrm{O}_3/\mathrm{O}_3$ is an increasing function of NO_x.

The lower panel of Figure 2 shows the fractional changes in OH, HO_2, NO, and NO_2 that are associated with the introduction of acetone. The fractional reductions in NO and NO_2 are largest at low NO_x, while the increases in OH and HO_2 increase rapidly with NO_x for NO_x larger than 300 pptv.

3. HO_x and NO_x Partitioning

The lower panel of Figure 2 shows that acetone favors the partitioning of HO_x to HO_2 and of NO_x to NO_2. This can be explained using the standard steady state expressions for the partitioning of HO_x and NO_x. Using the reaction labeling convention given in Appendix A, the OH/HO_2 ratio is approximately given by

$$\frac{[\mathrm{OH}]}{[\mathrm{HO_2}]} = \frac{k_5[\mathrm{O_3}] + k_6[\mathrm{NO}]}{k_7[\mathrm{O_3}] + k_8[\mathrm{CO}]}. \tag{4}$$

If the fractional changes in OH, HO_2, and NO are small, and it is assumed that the fractional changes in CO and O_3 associated with the introduction of acetone can be ignored, it can be shown that

$$\frac{d\mathrm{OH}}{\mathrm{OH}} = \frac{d\mathrm{HO_2}}{\mathrm{HO_2}} + f_{19}\frac{d\mathrm{NO}}{\mathrm{NO}}. \tag{5}$$

The fractional reaction rate f_{19} is defined in Appendix B as the relative likelihood that an HO_2 radical will react with NO as opposed to either NO or O_3. Its dependence on NO_x is shown in Figure 3.

The lower panel of Figure 4 compares dOH/OH in the model with the estimate given in (5). The agree-

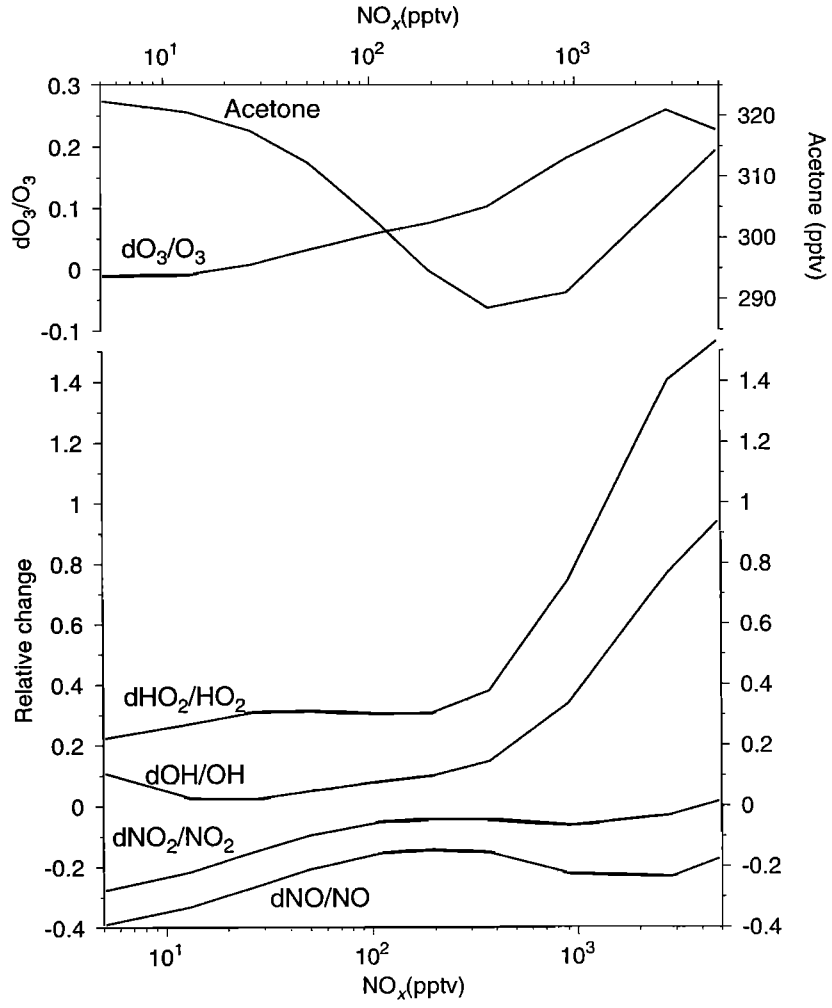

Figure 2. (bottom) Fractional changes in OH, HO_2, NO, and NO_2 from the baseline model run associated with the introduction of acetone into the model. (top) Fractional change in O_3 (ppbv) caused by the addition of acetone. Also shown is the acetone mixing ratio (pptv) in the model.

ment is quite good at low NO_x. The negative contribution of the dNO/NO term in (5) lowers $d\mathrm{HO_2}/\mathrm{HO_2}$ and brings the predicted dOH/OH closer to the modeled value. The agreement is poor at high NO_x.

The top panel of Figure 2 shows that $d\mathrm{O_3}/\mathrm{O_3}$ is not necessarily small. However, the variation of O_3 can be neglected in (5) because the fractional reaction rates that couple dOH/OH to $d\mathrm{O_3}/\mathrm{O_3}$ are small unless NO_x mixing ratios are extremely low, in which case $d\mathrm{O_3}/\mathrm{O_3}$ is small.

The standard expression for partitioning NO_x is

$$\frac{\mathrm{NO}}{\mathrm{NO_2}} = \frac{J_{\mathrm{NO_2}}}{k_9[\mathrm{O_3}] + k_6[\mathrm{HO_2}]}. \tag{6}$$

This yields a first-order relationship between dNO and $d\mathrm{NO_2}$ given by

$$\frac{d\mathrm{NO_2}}{\mathrm{NO_2}} = \frac{d\mathrm{NO}}{\mathrm{NO}} + f_{18}\frac{d\mathrm{HO_2}}{\mathrm{HO_2}} + (1 - f_{18})\frac{d\mathrm{O_3}}{\mathrm{O_3}}. \tag{7}$$

NO_2 is coupled to changes in HO_2 and O_3 via the fractional reaction rate f_{18}. The coupling of NO_2 to HO_2 is strongest at low NO_x where f_{18} is large (see Figure 3). NO_2 is most sensitive to changes in O_3 at high NO_x, where $(1\text{-}f_{18})$ is largest. The upper panel of Figure 4 compares the change in NO_2 predicted by (7) with the actual change of NO_2 in the model. Neglect of the $d\mathrm{O_3}/\mathrm{O_3}$ term in (7) would lead to substantial disagreement with modeled $d\mathrm{NO_2}/\mathrm{NO_2}$ at high NO_x. The full expression agrees quite well with $d\mathrm{NO_2}/\mathrm{NO_2}$ over the entire range of NO_x mixing ratios.

4. HO_x Budget

Steady state expressions for the partitioning of HO_x and NO_x are of some help in interrelating some of the changes in HO_x and NO_x caused by the introduction of HO_x sources. However, they cannot be used to predict the absolute response of HO_x to a HO_x source. This requires an analysis of the HO_x budget. The three most pervasive sources of HO_x to the upper troposphere are the $O^1D + H_2O$ reaction, methane oxidation, and acetone oxidation. Quantifying the size of the $O^1D + H_2O$ source is straightforward. However, both methane

and acetone have a large number of oxidation pathways, each of which will produce or destroy different numbers of HO_x. In a computer simulation it is difficult to determine from which hydrocarbon a HO_x originates because the oxidation pathways of methane and acetone have many intermediates in common. We show in Appendices C and D how a modified version of a previously introduced method [*Arnold et al.*, 1997] can be used to predict the HO_x yields of methane, acetone and their intermediates.

The HO_x yields of CH_3OOH and methane, calculated using the fractional reaction rates from the model and the expressions given in Appendix C, are plotted against the ambient NO_x mixing ratio in Figure 5. The HO_x yield of CH_3OOH is anticorrelated with the OH mixing ratio and varies between 1 and 2. Within the usual range of NO_x mixing ratios in the upper troposphere (10 pptv $\leq$ NO $\leq$ 100 pptv), it can be considered a decreasing function of NO_x. The HO_x yield of methane slowly increases with NO_x [see also *Müller and Brasseur*, 1999].

The HO_x yield of acetone was calculated using the method of Appendix D and is plotted against NO_x in Figure 5. It increases rapidly from 0.5 at $NO_x = 5$ pptv to 2.5 at $NO_x = 1000$ pptv. Also shown is the HO_x yield of acetone assuming the only sink is photolysis. Consideration of the OH channel significantly reduces the HO_x yield of acetone in the intermediate range of NO_x mixing ratios for which OH concentrations are largest. *Singh et al.* [1995] have demonstrated that the HO_x yield of acetone via the photolysis channel is 3.2 in the high NO_x limit. This approximation is quite accurate for $NO_x \geq 100$ pptv but significantly overestimates HO_x production from acetone for much of the observed range of NO_x mixing ratios in the upper troposphere [see also *Müller and Brasseur*, 1999].

The three main sources of HO_x in the model have been plotted against NO_x in Figure 6. The production of HO_x from methane oxidation ($PHO_x(CH_4)$) and from acetone oxidation (PHO_x(ACET)) have been calculated using (C1) and (D1). The dependence of $PHO_x(CH_4)$ on NO_x arises mainly from its dependence on [OH]. The variation in $PHO_x(O^1D+H_2O)$ with NO_x reflects its dependence on [O_3]. The increase in PHO_x(ACET) with NO_x occurs largely because the HO_x yield of acetone is an increasing function of NO_x. Also plotted in Figure 6 are $LHO_x(OH+HO_2)$ and $LHO_x(OH+NO_2)$, the dominant HO_x sinks at low and high NO_x, respectively. Not all HO_x sinks are shown. Formation of H_2O_2 is the second most impor-

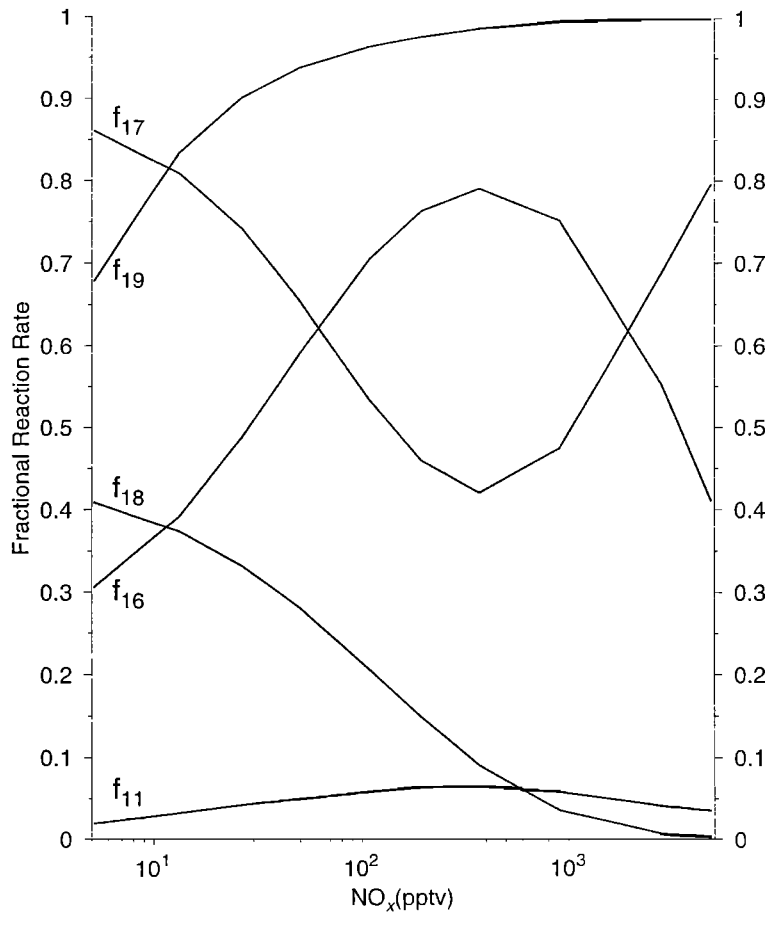

Figure 3. The dependence against NO_x of five fractional reaction rates: f_{17}, fraction of HNO_3 undergoing photolysis; f_{19}, fraction of HO_2 reacting with NO; f_{18}, fraction of NO reacting with HO_2; f_{16}, fraction of HNO_4 reacting with OH; and f_{11}, fraction of CH_3COO_2 reacting with NO_2.

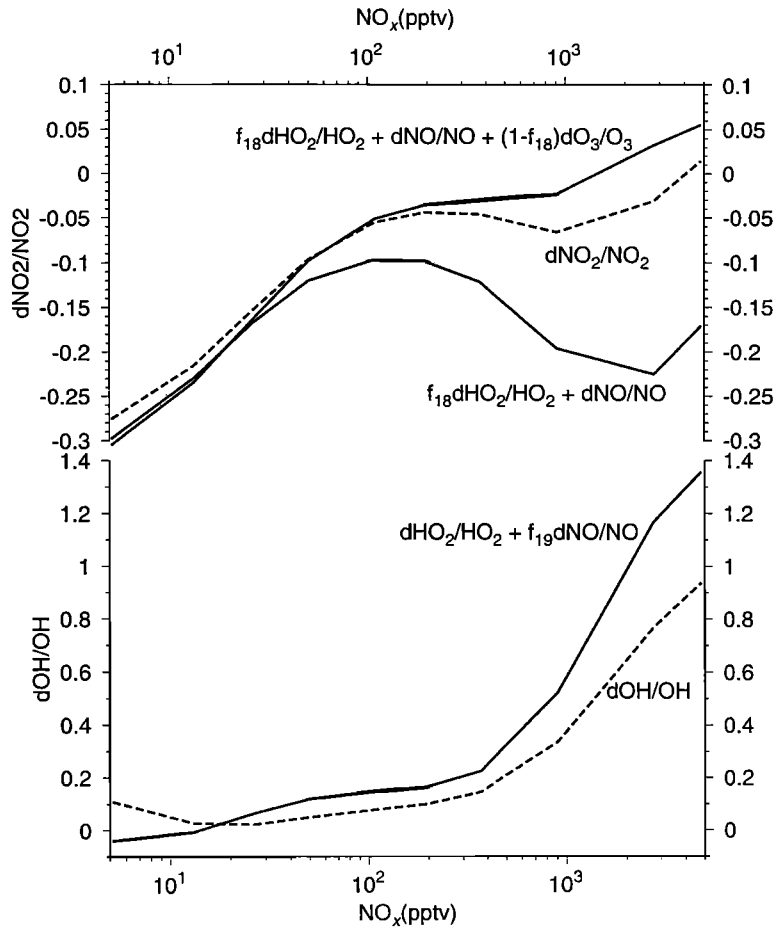

Figure 4. (bottom) The fractional change in OH from the introduction of acetone into the model compared with the change predicted by equation (5). (top) The fractional change in NO_2 from the introduction of acetone into the model compared with the change predicted by (7), with and without the contribution from the ozone response. The change in ozone has a strong effect on the change in NO_2 at high NO_x.

tant HO_x at low NO_x, where HO_2 concentrations are high. Formation of HNO_4 is important in an intermediate range of NO_x concentrations but goes to zero in both the low and high NO_x limits.

The complexity of the HO_x budget makes it difficult to predict the response of HO_x to acetone over the entire range of NO_x mixing ratios. We determine this response in the low and high NO_x limits. If there is no net change in HO_x over a day,

$$\mathrm{LHO}_x = \mathrm{PHO}_x. \tag{8}$$

In the absence of acetone and in the low NO_x limit,

$$k_{\mathrm{OH+HO_2}}[\mathrm{OH}][\mathrm{HO_2}] = \mathrm{PHO}_x(\mathrm{O}^1D + \mathrm{H_2O}) + \mathrm{PHO}_x(\mathrm{CH_4}). \tag{9}$$

The presence of acetone will introduce increases in $\mathrm{PHO}_x(\mathrm{O}^1D)$ that scale with $d\mathrm{O_3}/\mathrm{O_3}$ and increases in $\mathrm{PHO}_x(\mathrm{CH_4})$ that scale with $d\mathrm{OH}/\mathrm{OH}$. We assume that these changes in the HO_x budget are small compared with $\mathrm{PHO}_x(\mathrm{ACET})$. In that case,

$$k_{\mathrm{OH+HO_2}}[\mathrm{OH} + d\mathrm{OH}][\mathrm{HO_2} + d\mathrm{HO_2}] = \mathrm{PHO}_x + \mathrm{PHO}_x(\mathrm{ACET}). \tag{10}$$

To first order in $d\mathrm{OH}$ and $d\mathrm{HO_2}$, this gives under low NO_x

$$\frac{d\mathrm{OH}}{\mathrm{OH}} + \frac{d\mathrm{HO_2}}{\mathrm{HO_2}} = \frac{\mathrm{PHO}_x(\mathrm{ACET})}{\mathrm{PHO}_x}. \tag{11}$$

The right- and left-hand sides of (11) have been plotted against NO_x in Figure 7. There is reasonable agreement at low NO_x. Equation (11) gives some insight into why the impact of acetone on OH in the low NO_x limit is smaller than what one might anticipate. First, $d\mathrm{OH}/\mathrm{OH}$ is small because the the production of HO_x from acetone, normalized by the total unperturbed HO_x production, is constrained to equal the sum $d\mathrm{OH}/\mathrm{OH}$ + $d\mathrm{HO_2}/\mathrm{HO_2}$. Second, changes in HO_x partitioning arising from changes in NO constrain $d\mathrm{HO_2}/\mathrm{HO_2}$ to be larger than $d\mathrm{OH}/\mathrm{OH}$, which by (11) must reduce $d\mathrm{OH}/\mathrm{OH}$. Third, the HO_x yield of acetone is small at low NO_x.

A similar analysis can also be carried out in the high NO_x limit. Assume in the absence of acetone that

$$k_{OH+NO_2}[OH][NO_2] = PHO_x(O^1D + H_2O) + PHO_x(CH_4). \quad (12)$$

Acetone will then induce changes in OH and NO_2 such that

$$\frac{dOH}{OH} + \frac{dNO_2}{NO_2} = \frac{PHO_x(ACET)}{PHO_x}. \quad (13)$$

Figure 7 shows that there is excellent agreement between the two sides of this equation for $NO_x \geq 800$ pptv. In this limit, OH is quite sensitive to the introduction of acetone. This is partly because dNO_2/NO_2 is very small, so that dOH/OH is roughly equal to $PHO_x(ACET)/PHO_x$. The fractional contribution of acetone to the total HO_x production itself also increases with NO_x. This is because the HO_x yield of acetone increases with NO_x and because decreases in OH and O_3 at high NO_x reduce PHO_x.

5. Ozone Production

The five largest ozone production and destruction terms in the model were shown in Figure 1. The NO + HO_2 term is larger than the other four by about an order of magnitude. We will assume that most of the changes in ozone production from a HO_x source arise from changes in this term. The fractional change in $P(O_3)$ associated with the introduction of a HO_x source can then be approximated as

$$\frac{dP(O_3)}{P(O_3)} = \frac{dHO_2}{HO_2} + \frac{dNO}{NO}. \quad (14)$$

The validity of this approximation is assessed in Figure 8. The two sides of (14) agree well for $NO_x \leq 300$ pptv. They start to differ at high NO_x because the increasing magnitude of dHO_2/HO_2 undermines the validity of the linearized approach.

In the absence of changes in NO, the fractional change in $P(O_3)$ would equal the fractional change in HO_2. Figure 8 shows that $dP(O_3)/P(O_3)$ is substantially smaller than dHO_2/HO_2, especially when NO_x mixing ratios are less than 300 pptv. When NO_x is less than 25 pptv, the NO reduction is larger than the HO_2 increase, so that acetone gives rise to a net decrease in ozone production.

Perturbation theory can be used to help predict the response of $P(O_3)$ to a HO_x source if dNO/NO can be expressed in terms of dHO_2/HO_2. To do this, we

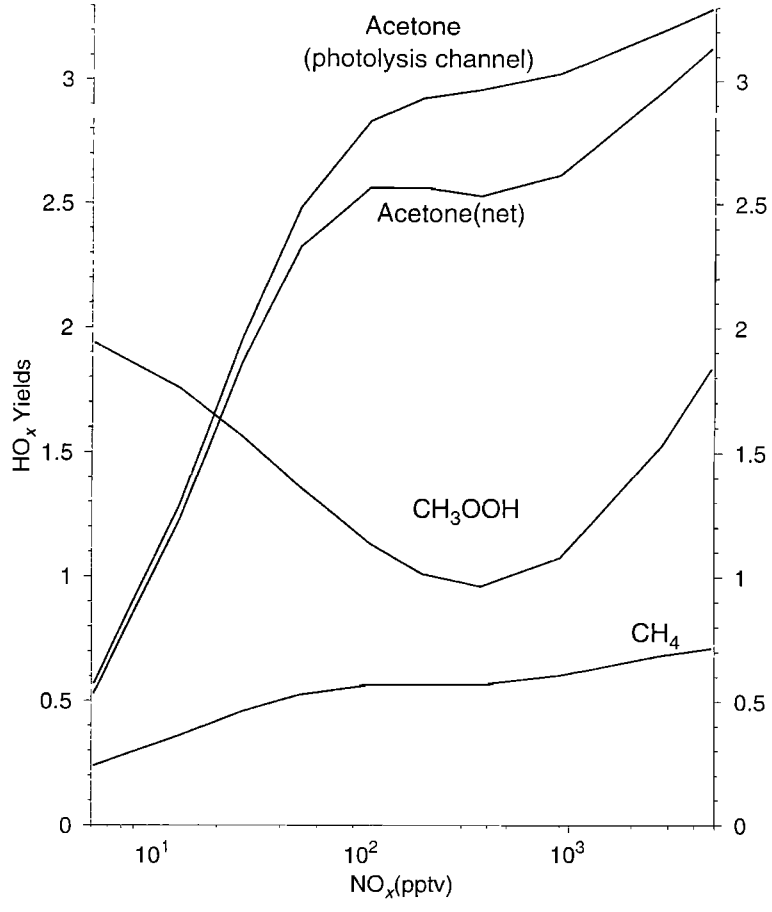

Figure 5. The HO_x yields of methane (CH_4), methyl hydroperoxide (CH_3OOH), acetone (OH attack and photolysis channels), and acetone (photolysis channel only), plotted against NO_x.

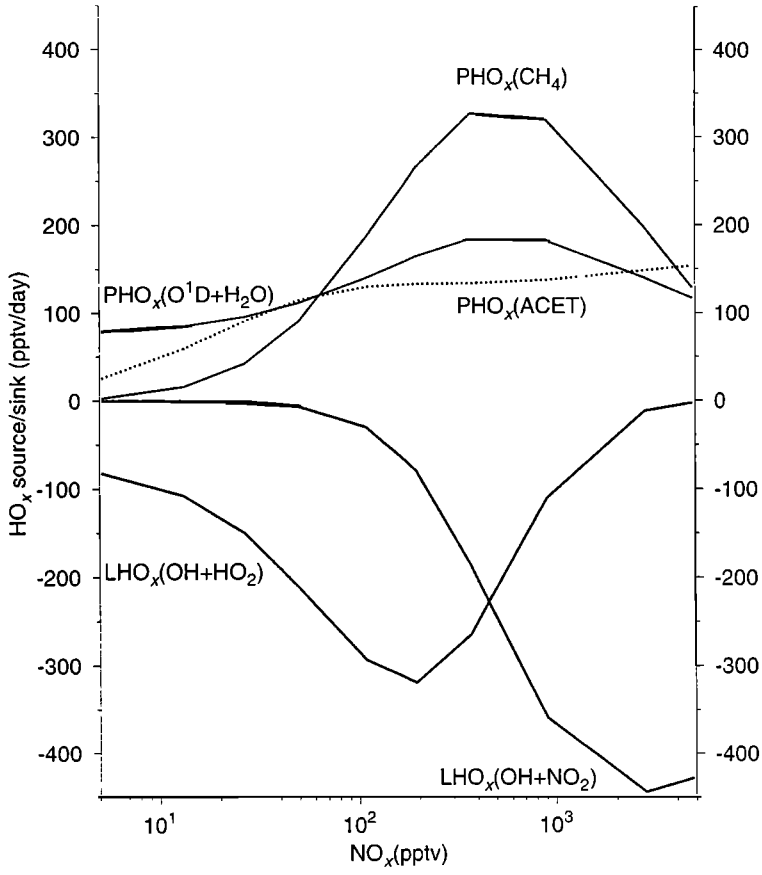

Figure 6. The dominant HO_x sources and sinks in the model plotted against NO_x. Each rate is a day average. PHO_x(ACET) is represented by the dotted line.

assume that the introduction of acetone results in an increased conversion of NO to NO_2, HNO_4 HNO_3, and PAN but to no other NO_y species.

$$NO\frac{dNO}{NO} + NO_2\frac{dNO_2}{NO_2} + HNO_4\frac{dHNO_4}{HNO_4} + HNO_3\frac{dHNO_3}{HNO_3} + dPAN = 0. \quad (15)$$

This expression implicitly assumes that the introduction of a HO_x source has no effect on the NO_y lifetime. The response of NO_2 to a HO_x source is given in (7). Those of HNO_4, HNO_3, and PAN can be obtained by again using the assumption of photochemical steady state.

The thermal decomposition of HNO_4 can be ignored in the upper troposphere. If the sources and sinks of HNO_4 are those given in Appendix A, it can be shown that

$$\frac{dHNO_4}{HNO_4} = \frac{dNO_2}{NO_2} + \frac{dHO_2}{HO_2} - f_{16}\frac{dOH}{OH}. \quad (16)$$

The fractional reaction rate f_{16} is defined in Appendix B. Its variation with NO_x is shown in Figure 3. The fractional change in HNO_4 predicted by (16) is compared with the actual fractional change of HNO_4 in the lower panel of Figure 9. The agreement is quite good.

If the sources and sinks of HNO_3 are those listed in Appendix B, then the change in HNO_3 can be approximated as

$$\frac{dHNO_3}{HNO_3} = \frac{dNO_2}{NO_2} + f_{17}\frac{dOH}{OH}, \quad (17)$$

where f_{17} is defined in Appendix B and plotted versus NO_x in Figure 3. The middle panel of Figure 9 compares the fractional change in HNO_3 predicted by (17) with the change in the model. The agreement is again very good, despite the long photochemical lifetime of HNO_3. Acetone reduces HNO_3 for NO_x less than 100 pptv, where the decrease in dNO_2/NO_2 more than offsets the increase in dOH/OH.

PAN is formed by the reaction between CH_3COO_2 and NO_2. The dominant source of CH_3COO_2 in the model is acetone photolysis. The dominant sink of PAN in the model is photolysis. At steady state,

$$f_{11}J_{ACET}[ACET] = J_{PAN}[PAN]. \quad (18)$$

In this expression, f_{11} represents the fractional reaction rate for the conversion of CH_3COO_2 to PAN. As is shown in Figure 3, this rate varies between 0.02 and 0.07 (i.e., 2-7% efficiency for the conversion of acetone to PAN). Since [PAN] = 0 in the baseline run, [PAN] = [dPAN], and

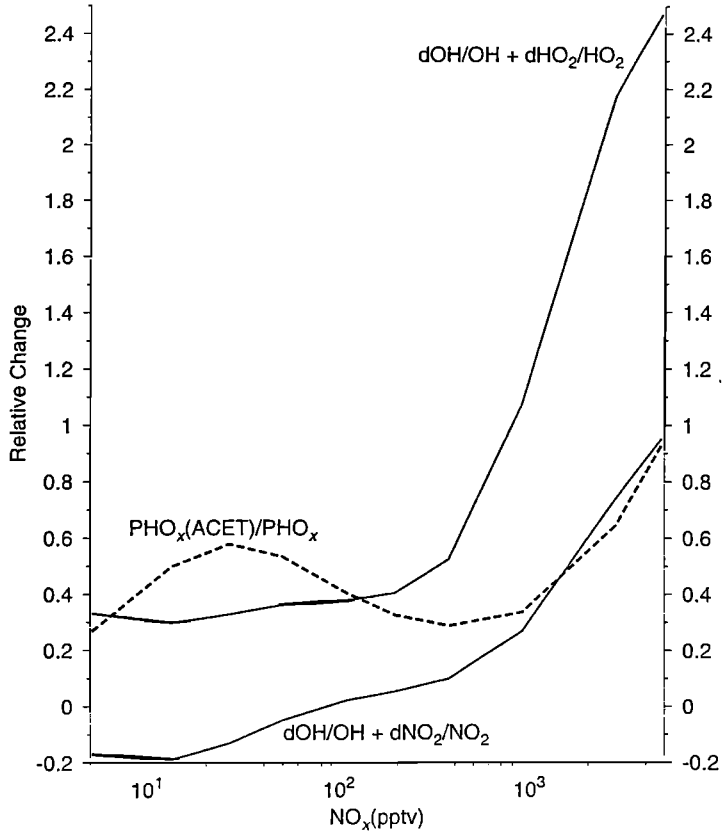

Figure 7. The dotted line represents the production of HO_x from acetone, normalized by the total production of HO_x in the baseline model. The two solid lines represent the sum of the fractional changes in OH and HO_2 and in OH and NO_2.

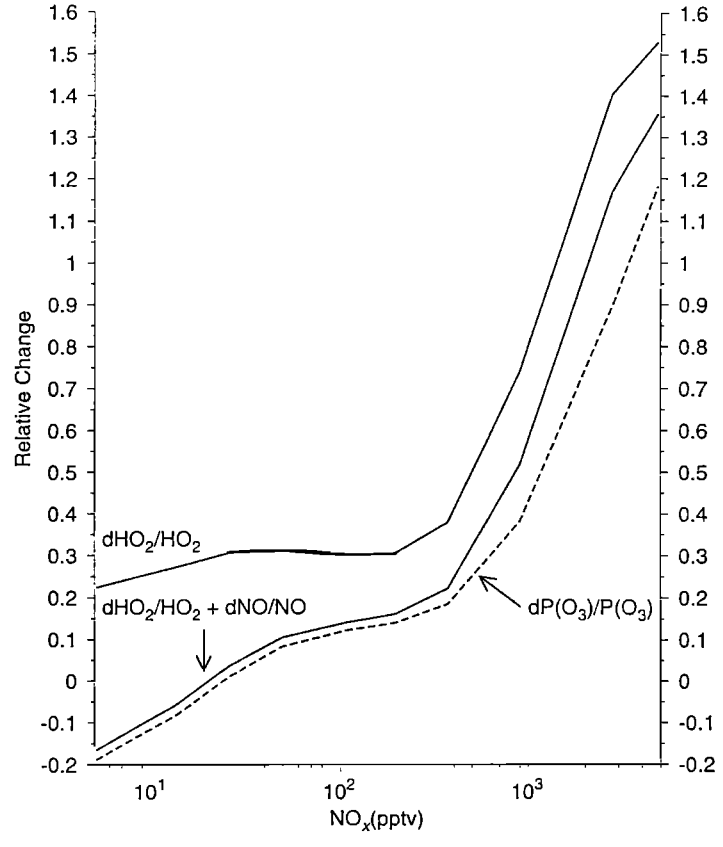

Figure 8. The fractional change in ozone production from adding acetone to the model (dashed line). Fractional changes in HO_2, and in HO_2 + dNO/NO (solid lines).

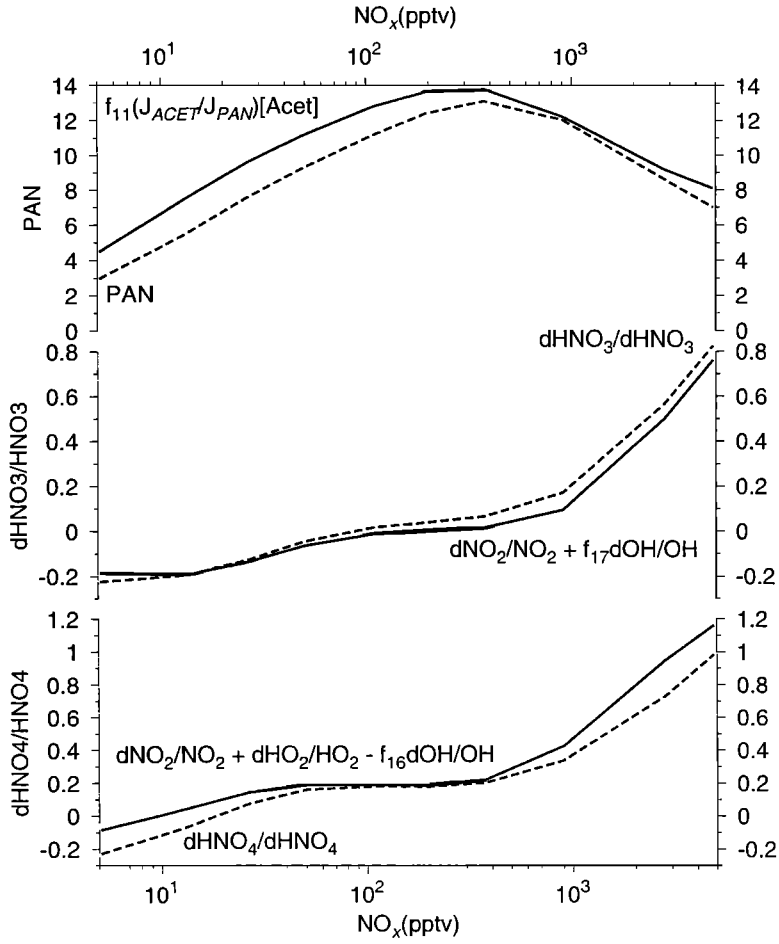

Figure 9. (bottom) The fractional change in HNO_4 from the introduction of acetone into the model (dotted line) compared with the change predicted by equation (16). (middle) The fractional change in HNO_3 from the introduction of acetone into the model (dotted line) compared with the change predicted by equation (17). (top) The change in peroxyacetylnitrate PAN from the introduction of acetone into the model (dotted line) compared with the change predicted by equation (19).

$$[d\mathrm{PAN}] = f_{11}\frac{J_{\mathrm{ACET}}}{J_{\mathrm{PAN}}}[\mathrm{ACET}]. \tag{19}$$

The top panel of Figure 9 compares the concentration of PAN predicted by this expression with the PAN in the model. Despite the long lifetime of PAN in the upper troposphere, the agreement is again quite good. PAN increases of between 4 and 14 pptv in the upper tropical troposphere from acetone are comparable with three-dimensional model results [*Singh et al.*, 1995].

In Figure 10 the changes in PAN, HNO_4, and HNO_3 from acetone have been normalized by the change in NO_x. PAN reduces NO_x most strongly at low NO_x, where it not only absorbs all of the NO_x decrease, but also lowers HNO_4 and HNO_3. Conversion of NO_x to HNO_3 dominates at large NO_x. Conversion to HNO_4 is important for intermediate NO_x mixing ratios.

If in (15) one substitutes (7) for $d\mathrm{NO_2}/\mathrm{NO_2}$ (dropping the $d\mathrm{O_3}/\mathrm{O_3}$ term because it proves to be unimportant), (16) for $d\mathrm{HNO_4}/\mathrm{HNO_4}$, (17) for $d\mathrm{HNO_3}/\mathrm{HNO_3}$, (19) for dPAN, and (5) for $d\mathrm{OH}/\mathrm{OH}$, one can write

$$\frac{d\mathrm{NO}}{\mathrm{NO}} = -\mathrm{R}\frac{d\mathrm{HO_2}}{\mathrm{HO_2}} - \frac{d\mathrm{PAN}}{\mathrm{R_{bot}}}. \tag{20}$$

The parameter R is given by

$$R = \frac{f_{18}\mathrm{NO_2} + \mathrm{HNO_4}(f_{18} + 1 - f_{16}) + \mathrm{HNO_3}(f_{18} + f_{17})}{\mathrm{NO} + \mathrm{NO_2} + \mathrm{HNO_4}(1 - f_{16}f_{19}) + \mathrm{HNO_3}(1 + f_{17}f_{19})}. \tag{21}$$

R helps estimate the decrease in NO from an increase in HO_2, associated with increased conversions of NO to NO_2, HNO_3, and HNO_4 (but not PAN). It could be used to estimate the fractional decrease in NO, from a given increase in HO_2, associated with a pure HO_x source such as CH_3OOH, which did not also produce PAN.

Figure 11 shows that R decreases steadily with NO_x. Ozone production from a pure HO_x source is therefore most heavily offset by decreases in NO at low NO_x. The decrease in R with NO_x is driven mainly by the decrease of f_{18} (shown in Figure 3).

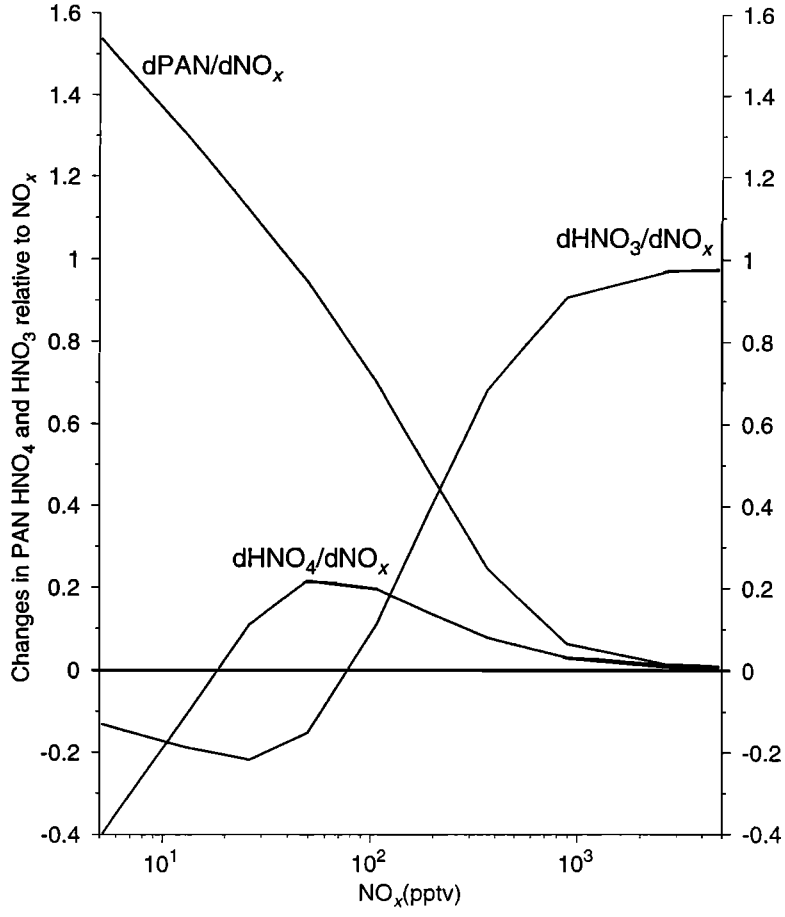

Figure 10. The changes in PAN, HNO_4, and HNO_3 from the introduction of acetone, normalized by the absolute change in NO_x.

The formation of PAN is also most effective at reducing ozone production at low NO_x. The NO reduction caused by conversion of NO to PAN is accounted for by the second term on the right-hand side of (20). The parameter R_{bot} in (20) is simply the denominator of the right-hand side of (21). It is roughly proportional to NO_x. Since dPAN is is only weakly dependent on NO_x (Figure 9), the relative reductions in NO from PAN are largest at small NO_x.

If one uses in (14) the expression for dNO/NO given by (20) and the expression for dPAN given in (19), the fractional change in $P(O_3)$ is given by

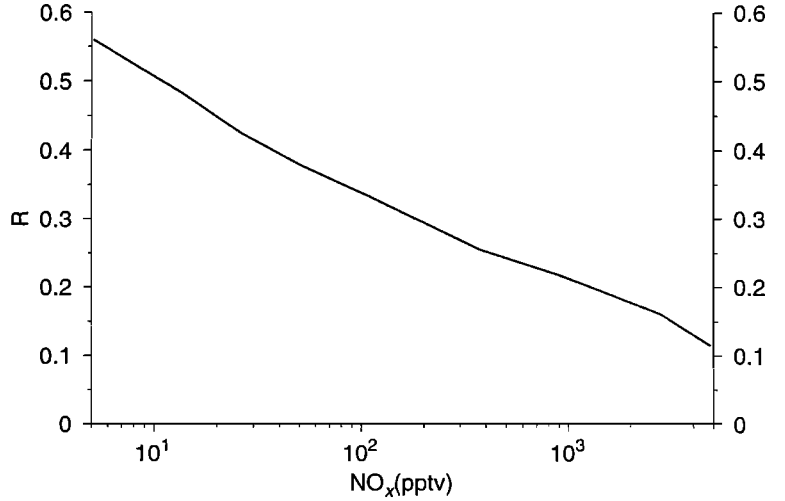

Figure 11. The variation with NO_x of the HO_x-NO_x coupling coefficient R as defined by equation (21) in the text.

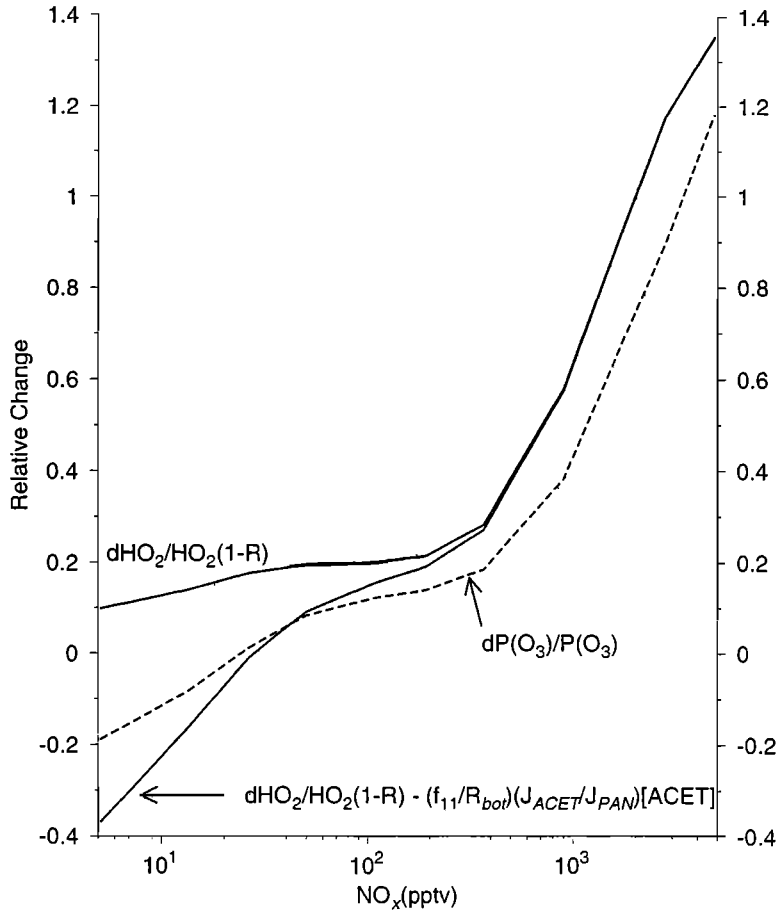

Figure 12. The fractional change in ozone production from adding acetone to the model (dashed line). The variation of $d\mathrm{HO_2}/\mathrm{HO_2}(1+\mathrm{R})$ and the change in ozone production predicted by equation (22), plotted against NO_x (solid lines).

$$\frac{d\mathrm{P(O_3)}}{\mathrm{P(O_3)}} = \frac{d\mathrm{HO_2}}{\mathrm{HO_2}}(1-R) - \frac{f_{11}}{R_{\mathrm{bot}}}\frac{J_{\mathrm{acet}}}{J_{\mathrm{PAN}}}[\mathrm{ACET}]. \quad (22)$$

This expression gives an estimate for the change in ozone production from a given change in HO_2 caused by acetone. For a HO_x source such as CH_3OOH that did not generate PAN, the second term on the right-hand side of (22) could be ignored. The two sides of (22) are compared in Figure 12. They agree reasonably well over a wide range of NO_x mixing ratios. The right-hand side of (22) underestimates ozone production at low NO_x because it overestimates PAN. The overestimate at high NO_x arises from the difference between $d\mathrm{P(O_3)}/\mathrm{P(O_3)}$ and $d\mathrm{NO}/\mathrm{NO}+d\mathrm{HO_2}/\mathrm{HO_2}$ shown in Figure 8. The right-hand side of (22) and $d\mathrm{HO_2}/\mathrm{HO_2}(1\text{-}R)$ both converge exactly to $d\mathrm{HO_2}/\mathrm{HO_2}$ + $d\mathrm{NO}/\mathrm{NO}$ in the high NO_x limit.

6. Summary

HO_x sources such as acetone increase OH and HO_2. But the relative size of these increases is highly dependent on the NO_x concentration. They will increase rapidly with NO_x when NO_x concentrations become larger than 300 pptv. This is driven by decreases in the strength of the other HO_x sources, by increases in the HO_x yield of acetone, and by changes in the chemistry of HO_x (self-buffered at low NO_x to NO_x-buffered at high NO_x). Errors in our assessment of HO_x sources and sinks will therefore give rise to the largest relative errors in model estimates of OH and HO_2 in the high NO_x regime. This may help account for a finding [*Faloona et al.*, 2000] that models tend to most strongly underestimate observed OH and HO_2 concentrations at high NO_x.

Acetone will usually increase ozone production in the upper troposphere because it increases HO_2. But this increase will be substantially offset by reduced concentrations of NO. These are driven by complex interactions between the HO_x and NO_y families which favor the partitioning of HO_x toward HO_2 and of NO_y from NO to more oxidized forms of nitrogen such as NO_2, HNO_3, HNO_4, and PAN. Much as with OH, the relative increase in ozone production from acetone will always increase with NO_x.

It should be kept in mind that although the relative increases in OH and ozone production from HO_x sources are largest in the high NO_x regime, the absolute increases in OH and ozone production from HO_x sources

will tend to be largest in the intermediate regime where OH and ozone production are maximized [*Folkins et al.*, 1998].

Linear theory provides insight into some of the complex feedbacks that occur in the photochemistry of the atmosphere when it is subject to a perturbation such as a HO_x source. There is nothing in this approach that restricts its applicability only to changes in the concentrations of HO_x sources. It should therefore be useful in predicting the first-order chemical response of the atmosphere to the introduction of other trace species.

Appendix A: Reaction Constants

This is a list of the reaction constants needed to define the fractional reaction rates.

k_1 $HO_2 + NO_2 + M \rightarrow HNO_4 + M$
k_2 $OH + HNO_4 \rightarrow$ products
k_3 $OH + NO_2 + M \rightarrow HNO_3 + M$
k_4 $OH + HNO_3 \rightarrow H_2 + NO_3$
k_5 $HO_2 + O_3 \rightarrow OH + 2O_2$
k_6 $NO + HO_2 \rightarrow NO_2 + OH$
k_7 $OH + O_3 \rightarrow HO_2 + O_2$
k_8 $CO + OH(+O_2) \rightarrow CO_2 + HO_2$
k_9 $NO + O_3 \rightarrow NO_2 + O_2$
k_{10} $NO + CH_3O_2 \rightarrow NO_2 + CH_3O$
k_{11} $O^1D + H_2O \rightarrow 2\,OH$
k_{12} $CH_2O + OH(+O_2) \rightarrow CO + HO_2 + H_2O$
k_{13} $CH_3OOH + OH \rightarrow 0.7CH_3O_2 + 0.3(CH_2O + OH) + H_2O$
k_{14} $CH_3O_2 + NO(+O_2) \rightarrow CH_2O + HO_2 + NO_2$
k_{15} $CH_3O_2 + HO_2 \rightarrow CH_3OOH$
k_{16} $CH_4 + OH(+O_2) \rightarrow CH_3O_2 + H_2O$
k_{17} $CH_3COCH_3 + OH(+O_2) \rightarrow CH_3COCH_2OO$
k_{18} $CH_3COCH_2OO + NO(+O_2) \rightarrow CH_3COO_2 + CH_2O + NO_2$
k_{19} $CH_3COO_2 + NO_2 + M \rightarrow CH_3CO_2NO_2$ (PAN) $+ M$
k_{20} $CH_3COO_2 + NO(+O_2) \rightarrow CH_3O_2 + CO_2 + NO_2$
k_{21} $CH_3COO_2 + HO_2 \rightarrow 0.5(CH_3C(O)OOH + O_2) + 0.5(CH_3C(O)OH + O_3)$
k_{22} $CH_3C(O)OOH + OH \rightarrow CH_3COO_2 + H_2O$
k_{23} $CH_3COOH + OH \rightarrow CH_3O_2 + CO_2 + H_2O$
J_{NO_2} $NO_2 + h\nu \rightarrow NO + O$
J_{HNO_3} $HNO_3 + h\nu \rightarrow NO_2 + OH$
J_{HNO_4} $HNO_4 + h\nu \rightarrow NO_2 + HO_2$
J_{CH_2Oa} $CH_2O + h\nu(+2O_2) \rightarrow CO + 2HO_2$
J_{CH_2Ob} $CH_2O + h\nu \rightarrow CO + H_2$
J_{CH_3OOH} $CH_3OOH + h\nu \rightarrow OH + HO_2 + CH_2O$
J_{ACET} $CH_3COCH_3 + h\nu(+2O_2) \rightarrow CH_3COO_2 + CH_3O_2$
J_{PAN} $CH_3CO_2NO_2 + h\nu(+2O_2) \rightarrow CH_3COO_2 + NO_2$
$J_{CH_3C(O)OOH}$ $CH_3C(O)OOH + h\nu \rightarrow CH_3O_2 + OH + CO_2$

Appendix B: Fractional Reaction Rates

$f_1 = J_{CH_2Oa}/(J_{CH_2Oa} + J_{CH_2Ob} + k_{12}[OH])$
$f_2 = J_{CH_2Ob}/(J_{CH_2Oa} + J_{CH_2Ob} + k_{12}[OH])$
$f_3 = k_{12}[OH]/(J_{CH_2Oa} + J_{CH_2Ob} + k_{12}[OH])$
$f_4 = J_{CH_3OOH}/(J_{CH_3OOH} + k_{13}[OH])$
$f_5 = k_{13}[OH]/(J_{CH_3OOH} + k_{13}[OH])$
$f_6 = k_{14}[NO]/(k_{15}[HO_2] + k_{14}[NO])$
$f_7 = k_{15}[HO_2]/(k_{15}[HO_2] + k_{14}[NO])$
$f_8 = J_{ACET}/(J_{ACET} + k_{17}[OH])$
$f_9 = k_{17}[OH]/(J_{ACET} + k_{17}[OH])$
$f_{10} = k_{20}[NO]/(k_{19}[NO_2] + k_{20}[NO] + k_{21}[HO_2])$
$f_{11} = k_{19}[NO_2]/(k_{19}[NO_2] + k_{20}[NO] + k_{21}[HO_2])$
$f_{12} = 0.5k_{21}[HO_2]/(k_{19}[NO_2] + k_{20}[NO] + k_{21}[HO_2])$
$f_{13} = f_{12}$
$f_{14} = k_{22}[OH]/(J_{CH_3C(O)OOH} + k_{22}[OH])$
$f_{15} = J_{CH_3C(O)OOH}/(J_{CH_3C(O)OOH} + k_{22}[OH])$
$f_{16} = k_2[OH]/(J_{HNO_4} + k_2[OH])$
$f_{17} = J_{HNO_3}/(J_{HNO_3} + k_4[OH])$
$f_{18} = k_6[HO_2]/(k_9[O_3] + k_6[HO_2])$
$f_{19} = k_6[NO]/(k_5[O_3] + k_6[NO])$

Appendix C: HO_x Yield of Methane

An overview of methane oxidation is given in Figure 13. The main sink of CH_4 is OH attack. Although this reaction destroys one HO_x, subsequent reactions almost invariably result in a net production of HO_x. If $HY(CH_4)$ is the net number of HO_x produced or destroyed during an OH-initiated oxidation of CH_4, then the rate of HO_x production from CH_4 oxidation can be written

$$PHO_x(CH_4) = k_{OH+CH_4}[OH][CH_4]HY(CH_4). \quad (C1)$$

Since one HO_x is used to produce CH_3O_2 from CH_4, the HO_x yield of CH_4 can be simply related to the HO_x yield of the methyl peroxy radical (CH_3O_2):

$$HY(CH_4) = HY(CH_3O_2) - 1. \quad (C2)$$

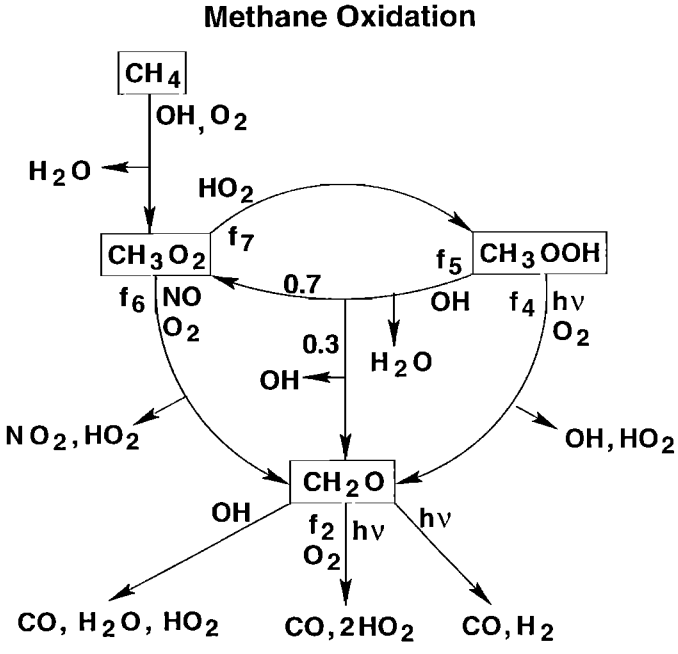

Figure 13. An overview of methane (CH_4) oxidation.

CH_3O_2 can react either with NO or HO_2. Defining f_6 and f_7 as the fractional reaction rates for the two possibilities respectively, the HO_x yield of CH_3O_2 can be written

$$\mathrm{HY(CH_3O_2)} = f_6[\mathrm{HY(CH_2O)} + 1] + f_7[\mathrm{HY(CH_3OOH)} - 1]. \quad \text{(C3)}$$

The HO_x yield of formaldehyde is simply

$$\mathrm{HY(CH_2O)} = 2f_1, \quad \text{(C4)}$$

where f_1 is a fractional reaction rate for the photolysis of CH_2O producing two HO_2. The other two sinks of CH_2O considered in Figure 13 are HO_x neutral.

If f_4 and f_5 represent the fractional reaction rates of CH_3OOH via photolysis and OH attack,

$$\mathrm{HY(CH_3OOH)} = f_4[\mathrm{HY(CH_2O)} + 2] + f_5[0.3\mathrm{HY(CH_2O)} + 0.7\mathrm{HY(CH_3O_2)} - 0.7] \quad \text{(C5)}$$

The four constraints (C2) through (C5) can be used to solve for the HO_x yields of CH_4, CH_2O, CH_3O_2, and CH_3OOH. The HO_x yield of CH_3OOH is given by

$$\mathrm{HY(CH_3OOH)} = \frac{[2f_4(1+f_1) + f_5(0.6f_1 - 0.7) + 0.7f_5f_6(1+2f_1) - 0.7f_5f_7]}{(1 - 0.7f_5f_7)}. \quad \text{(C6)}$$

The HO_x yield of CH_4 can be obtained by using (C3), (C4), and (C6) in (C2).

Appendix D: HO_x Yield of Acetone

An overview of acetone oxidation is shown in Figure 14. The two major sinks of acetone are photolysis and OH attack. The rate of HO_x production from acetone oxidation can be written

$$\mathrm{PHO}_x\mathrm{(ACET)} = (J_{\mathrm{ACET}} + k_{17}[\mathrm{OH}])[\mathrm{ACET}]\mathrm{HY(ACET)}. \quad \text{(D1)}$$

If f_8 and f_9 represent the fractional reaction rates for photolysis and OH attack,

$$\mathrm{HY(ACET)} = f_8(\mathrm{HY(CH_3O_2)} + \mathrm{HY(CH_3COO_2)}) + f_9(\mathrm{HY(CH_2O)} + \mathrm{HY(CH_3COO_2)} - 1). \quad \text{(D2)}$$

Appendix C shows how to evaluate $HY(CH_3O_2)$ and $HY(CH_2O)$. We assume PAN is stable. Use PAA (peracetic acid) to denote $CH_3C(O)OOH$ and AA (acetic acid) to denote $CH_3C(O)OH$. The HO_x yield of the CH_3COO_2 radical is given by

$$\mathrm{HY(CH_3COO_2)} = f_{10}\mathrm{HY(CH_3O_2)} + f_{12}(\mathrm{HY(PAA)} - 1) + f_{13}(\mathrm{HY(AA)} - 1). \quad \text{(D3)}$$

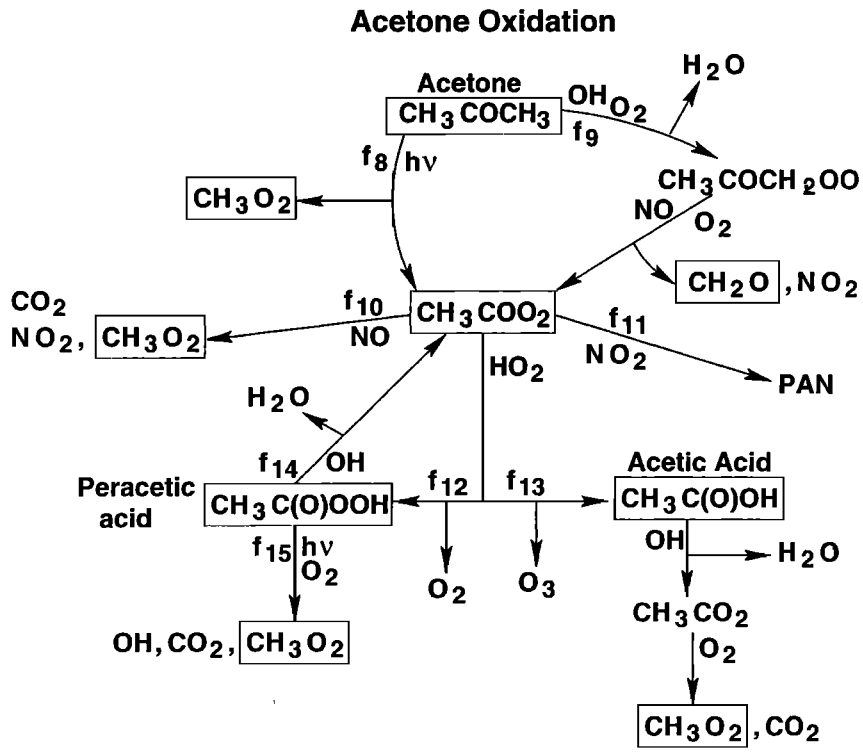

Figure 14. An overview of acetone (CH_3COCH_3) oxidation. One simplification has been to ignore the reaction of $CH_3COCH_2O_2$ with HO_2. There is little kinetic information available on this reaction, but it can be estimated to be competitive with the NO reaction only for NO $\leq$ 20 pptv.

The HO_x yield of PAA can be written

$$\begin{aligned} HY(PAA) &= f_{14}(HY(CH_2COO_2) - 1) \\ &+ f_{15}(HY(CH_3O_2) + 1). \end{aligned} \quad (D4)$$

The HO_x yield of AA can be written

$$HY(AA) = HY(CH_3O_2) - 1. \quad (D5)$$

These equations can be used to show that

$$HY(CH_3COO_2) = \frac{[HY(CH_3O_2)(f_{10} - f_{12}f_{15} + f_{13}) - 2f_{13}]}{(1 - f_{12}f_{14})}. \quad (D6)$$

The HO_x yield of acetone can then be determined by using (D6) and the known HO_x yields of CH_3O_2 and CH_2O in (D2).

Acknowledgments. This research was supported by the Natural Sciences and Engineering Council of Canada. R. Chatfield acknowledges the support of grant 622-61-10-10 from NASA's Global Tropospheric Experiment, with model development aided by the Modeling and Analysis Program, grant 622-59-39-10.

References

Arnold, F., V. Burger, B. Droste-Fanke, F. Grimm, A. Krieger, J. Schneider, and T. Stilp, Acetone in the upper troposphere and lower stratosphere: Impact on trace gases and aerosols, *Geophys. Res. Lett., 24,* 3017-3020, 1997.

Chatfield, R. B., and P. J. Crutzen, Sulfur dioxide in remote oceanic air: Cloud transport of reactive precursors, *J. Geophys. Res., 89,* 7111-7132, 1984.

Chatfield, R. B., J. A. Vastano, H. B. Singh, and G. Sachse, A general model of how fire emissions and chemistry produce African/oceanic plumes (O_3, CO, PAN, smoke) in TRACE A, *J. Geophys. Res., 101,* 24,279-24,306, 1996.

Faloona, I. , et al., Observations of HO_x and its relationship with NO_x in the upper troposphere during SONEX, accepted in *J. Geophys. Res., 105,* 3771-3783, 2000.

Folkins, I., P. O. Wennberg, T. F. Hanisco, J. G. Anderson, and R. J. Salawitch, OH, HO_2, and NO in two biomass burning plumes: Sources of HO_x and implications for ozone production, *Geophys. Res. Lett., 24,* 3185-3188, 1997.

Folkins, I. A., R. Chatfield, H. Singh, Y. Chen, and B. Heikes, Ozone production efficiencies of acetone and peroxides in the upper troposphere, *Geophys. Res. Lett., 25,* 1305-1308, 1998.

Jacob, D. J., et al., Origin of ozone and NO_x in the tropical troposphere: A photochemical analysis of aircraft observations over the South Atlantic basin, *J. Geophys. Res., 101,* 24,235-24,250, 1996.

Jaeglé, L., et al., Observed OH and HO_2 in the upper troposphere suggest a major source from convective injection of peroxides, *Geophys. Res. Lett., 24,* 3181-3184, 1997.

Jaeglé, L., D. J. Jacob, Y. Wang, A. J. Weinheimer, B. A. Ridley, T. L. Campos, G. W. Sachse, and D. E. Hagen, Sources and chemistry of HO_x in the upper troposphere over the United States, *Geophys. Res. Lett., 25,* 1705-1708, 1998.

Keim, E. R. et al., NO_y partitioning from measurements of nitrogen and hydrogen radicals in the upper troposphere, *Geophys. Res. Lett., 26,* 51-54, 1999.

McKeen, S. A., T. Gierczak, J. B. Burkholder, P. O. Wennberg, T. F. Hanisco, E. R. Keim, R.-S. Gao, S. C. Liu, A. R. Ravishankara, and D. W. Fahey, The photochemistry of acetone in the upper troposphere: A source of odd-hydrogen radicals, *Geophys. Res. Lett., 24,* 3177-3180, 1997.

Müller, J. F., and G. Brasseur, Sources of upper tropospheric HO_x: A three-dimensional study, *J. Geophys. Res., 104,* 1705-1715, 1999.

Prather, M. J., and D. J. Jacob, A persistent imbalance in HO_x and NO_x photochemistry of the upper troposphere driven by deep tropical convection, *Geophys. Res. Lett., 24,* 3189-3192, 1997.

Singh, H. B., M. Kanakidou, P. J. Crutzen, and D. J. Jacob, High concentration and photochemical fate of oxygenated hydrocarbons in the global troposphere, *Nature, 378,* 50-54, 1995.

Wennberg, P. O., et al., Hydrogen radicals, nitrogen radicals, and the production of ozone in the upper troposphere, *Science, 279,* 49-53, 1998.

R. Chatfield, Earth Science Division, NASA Ames Research Center, MS 245-5, Moffett Field, CA 94035. (chatfield@clio.arc.nasa.gov)

I. Folkins, Department of Oceanography, Dalhousie University, Halifax, Nova Scotia, Canada B3H 4J1. (Ian.Folkins@dal.ca)

(Received October 22, 1999; revised January 20, 2000; accepted January 27, 2000.)